FACULTY
OF MATHEMATICS
AND PHYSICS
Charles University

Electronic Transport Through Atoms and Molecules: Quantum Size-Effects and Strong Correlation

Habilitation Thesis

Ing. Richard Korytár, Ph.D.

March 2025

Abstract

This habilitation thesis summarizes my theoretical works in the field of electronic transport through molecular junctions and atomic adsorbates. Special focus is given to nanoscale conductors with a basic repeating unit: oligomers and atomic chains. In these systems, the observables show an interesting dependence on the number of units. Such effects are called quantum size-effects, since they stem from the underlying quantum nature of electrons. A subset of presented size-effects can be understood assuming effectively independent electronic degrees of freedom (quasi-particles). In some cases, the phenomena require a many-body strongly-correlated description. The thesis contains two parts: an introductory part, giving necessary background information and explaining wider research context and the second part with reprints of 25 publications.

Acknowledgment

The thesis would certainly never arise without mentors and experienced theorists: N. Lorente, F. Evers and T. Novotný. They provided support, inspiration and unfiltered critical opinion of my work. I am deeply grateful for the numerous international collaborations with all my co-authors–it was both enjoyable and unforgettable. I acknowledge the Czech Science foundation (Project No. 22-22419S) and the PRIMUS/Sci/09 program of Charles University for financial support of my work.

I am grateful for my colleagues at the institutions where I worked for their good humor, help and patience with my manners. Finally, I would like to thank my friends and family for their unwavering support through life's ups and downs.

Contents

List of Acronyms

AIM Anderson impurity model

CISS Chirality-induced spin selectivity

CIPA Coherent independent-particle approach

DFT Density functional theory

DMRG Density-matrix renormalization group

HOMO Highest occupied molecular orbital

KS Kohn-Sham

LDOS Local density of states

LUMO Lowest unoccupied molecular orbital

MCBJ Mechanically-controlled break-junction

Oac Oligoacenes

SIAM Single-impurity Anderson model

SMM Single-molecule magnet

STAIT Standard theory of *ab-initio* electron transport

STM Scanning-tunneling microscope

w.r.t. with respect to

List of frequently occurring physical quantities

$\mathrm{d}I/\mathrm{d}V$ derivative of the tunneling current

Δ_g Lowest excitation energy (gap) of a molecule

E_F Fermi energy

λ_F Fermi wavelength

k_F Fermi wavenumber

G Conductance

G_0 Conductance quantum, $= \frac{2e^2}{h}$

N Number of repeating units

T Temperature

$\mathcal{T}(E)$ Transmission probability

T_K Kondo temperature

U Coulomb integral (charging energy)

Foreword

This habilitation thesis summarizes my theoretical work in the field of quantum transport of electrons through nanoscale contacts. As the title suggests, the emphasis is on quantum size-effects and electronic correlation in atomic and molecular contacts. The thesis contains two parts: The second part is a collection of 25 associated articles (reprints) published in peer-reviewed journals. The first part (called short version), serves as an introduction to these associated articles. The objective of the first part is to give the reader background information, including: the main ideas of theoretical approaches employed, the most important Hamiltonians and other significant formulæ and a wider context of the research field.

In most cases, I am either the first, the last, or the second author of the associated articles. It is a common practice in theoretical-experimental collaborations to list the theoretical workhorse at the second place. Therefore, in these articles my role was essential and they would not be accomplished in the present form without my work and dedication. The remainder of the associated articles are authored by larger collaborations. In such cases, I honestly stated my contribution to these works. The associated works also show the gradual transition from the first authorship (as a postdoc) to the last authorship, *i.e.* to the stage of an independent researcher and a principal investigator of research grants.

The earliest works emerged during my three-year postdoc fellowship at KIT (Karlsruhe Institute of Technology), 2011-2014. I had entered this fellowship with a prior knowledge of Kondo systems and many-body physics from my Ph.D. thesis (at UÀB Barcelona), supervised by Nicolás Lorente. Some associated works followed from an ongoing collaboration with Nicolás. My main task at KIT as a postdoc was to learn *ab-initio* electronic transport theory, which resulted in very fruitful collaborations with some of the most renowned experimental labs (L. Venkataraman at Columbia University, O. Tal at Weizman Institute, W. Wulfhekel at KIT, etc.). At KIT I knew my lifelong mentor Ferdinand Evers, with whom I continued in my second postdoc at the Universtät Regensburg. In 2017 I became a senior scientist at the Charles University (Dept. of Condensed Matter Physics) in the group of Tomáš Novotný,

where I researched as an independent scientist. One article was co-written with my former doctoral student Štěpán Marek.

The associated publications are referenced with the word Article prepended, *i.e.* [Article 1] and ordered chronologically. This is to be contrasted with other references, where I used the usual style, *e.g.* [24]. The first part of the thesis attempts to give a certain logical structure for the list of associated works. Another way of organizing the list of articles is shown here:

1. **Theory: development and applications** [Article 25, Article 12, Article 13, Article 6, Article 3, Article 1, Article 2, Article 16, Article 21, Article 19, Article 24, Article 23]

2. **Theory-experiment collaborations** [Article 22, Article 4, Article 8, Article 18, Article 11, Article 10, Article 7, Article 5, Article 15, Article 14, Article 20, Article 9]

3. **A large review** [Article 17]

1 A brief overview of quantum transport of electrons in single-molecule and atomic junctions

In this chapter I give a brief overview of quantum transport through nanoscale conductors. The overview is not intended to be general; rather, it introduces foundational concepts that are common to most articles in this thesis.

First, physical systems of interest and associated observables are described in Sec. 1.1. This short section can serve as a proper introduction to this thesis. In further sections, most important theoretical concepts and models are given in a bit more more detail.

1.1 Introduction: Physical systems and their observables

One of the most fascinating achievements in physics in the last decades is the ability to perform measurements on a single atom or a single molecule. Of interest in this thesis are atoms and molecules 'wired' into an electric circuit. A voltage applied across the atomic-scale region causes electric current flow (Fig. 1.1). The current is the principal observable characteristic of these circuits.

Most of my theoretical works in this thesis aim to predict and interpret measurements from two major experimental approaches: scanning-tunneling microscopy (STM) and mechanically-controlled break-junction (MCBJ). For more details I suggest Refs. [1, 2, 3] and the review [Article 17].

Apart from the current-voltage response, other observables result from these techniques, such as equilibrium geometries and forces of the attached atom or molecule.

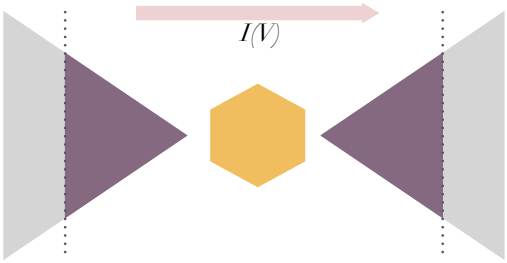

Figure 1.1: Scheme of a typical device for electron transport. The center (hexagon) represents a molecule or a single atom. It is contacted by the left and right leads (electrodes), also called source and drain. The voltage, which drives the electron current $I(V)$, is determined by the difference in their chemical potentials. Electrons in the central region and adjacent parts of the leads (between the two dotted lines) need to be treated fully quantum-mechanically. The outer part (reservoirs) can be treated in a simplified way. The theoretical predictions should not depend on the placement of the dotted lines.

As a side-note, I mention that the combined information of molecular conductance and a response of a molecule's geometry to the current opens up the possibility of investigating a molecular motor. My work in this direction is mentioned in the Outlook, Sec. 4.1.

1.2 Theoretical background

As outlined in the previous section, the principal observable of the transport setups is the electronic current in a stationary non-equilibrium caused by voltage bias (Fig. 1.1). A quantum-mechanical approach could therefore start straight with the time-dependent all-electron Schrödinger equation and evaluate the expectation values of the current density operator. It is a common situation in condensed matter physics that this agenda can not be pursued from first principles because of the vast number of degrees of freedom and their complexity. Some intricate aspects of this problem are

- The quantum-statistical density operator is not an equilibrium one
- Broken translational invariance impedes the use of Bloch's theorem. Electronic degrees of freedom couple at different length scales: Localized molecular degrees of freedom couple with extended degrees of freedom of the electrodes.
- Lack of Coulomb screening can lead to pronounced interaction effects

Section 1.2.1 reviews a formalism based on the assumption that charge transport is carried by effectively non-interacting electrons, *i.e.* particles of charge $-|e|$ that are subject to all force fields except their mutual interaction. This is a commonly adopted assumption in the transport theory of metallic systems because of efficient interaction screening that allows a quasi-particle description of charged elementary excitations. The formalism is denoted here CIPA or coherent independent-particle approach.

It is known from mesoscopic physics that quasiparticle relaxation effects are negligible at lengths smaller than the phase relaxation length L_Φ [4]. In typical leads like Au $L_\Phi \approx 1\mu$m at 1K [5]. In the molecular/atomic bridge, the CIPA breaks down if two effects are present:

1. The lack of screening could result in electron-electron interaction becoming dominant. The effects of strong correlation are especially prominent in the regime of so called *Coulomb blockade*.

2. Along with electronic wavefunctions, vibrational states localize as well. A typical 15 Å long molecule has vibrational level spacing of the order of 1 meV. Vibrational effects manifest in the electronic transport if the corresponding electron-vibrational coupling becomes strong.

In Sec. 1.2.1 I detail the CIPA. In Sec. 1.2.2 a parent model for certain correlation effects beyond CIPA is introduced.

1.2.1 Coherent independent-particle approach: Caroli formula

The formula for the electric current at voltage V applied to the junction adopts a very intuitive form

$$I(V) = \frac{2e}{h} \int \Big[n_{\mathrm{F}}(E - \mu_{\mathfrak{L}}(V)) - n_{\mathrm{F}}(E - \mu_{\mathfrak{R}}(V)) \Big] \mathcal{T}(E, V)\, \mathrm{d}E\,. \tag{1.1}$$

The integration represents summation over eigenstates of the independent-electron Hamiltonian of the complete system (atomic/molecular junction and the contacts). At each energy E the current is proportional to the transmission probability $\mathcal{T}(E, V)$. The latter can be viewed in analogy with transmission through electromagnetic waveguides; the Helmoltz equation is replaced by the single-electron Schrödinger equation. In contrast to waveguides, electrons obey Pauli principle. The latter is embedded by the difference between the Fermi-Dirac distributions $n_{\mathrm{F}}(E - \mu_{\mathfrak{L}}(V)) -$

$n_{\mathrm{F}}(E-\mu_{\mathfrak{R}}(V))$ of the left and right reservoirs. The difference between the left and right chemical potentials is the external voltage bias: $\mu_{\mathfrak{L}}(V)-\mu_{\mathfrak{R}}(V)=eV$. Equal temperatures of the reservoirs are assumed.

At zero temperature, we can readily obtain Landauer's formula for linear conductance [4]

$$G = G_0 \mathcal{T}(E_{\mathrm{F}}).$$

The conductance quantum $G_0 \coloneqq \frac{2e^2}{h}$ is evidently the conductance of a single transparent channel, *i.e.* when $\mathcal{T}(E)=1$.

Quantum nature of electrons appears in three different aspects in the Eq. (1.1): (1) the Pauli principle, (2) the transmission probability, determined by the single-particle Schrödinger equation and (3) the pre-factor of the integral. The inverse Planck's constant h^{-1} essentially converts energy (this is the physical unit of the integral) to rate. As it is known from scattering theory, there is an uncertainty principle that relates a decay rate of a metastable state to the spread in energy. The Eq. (1.1) can be viewed as a rate (inverse lifetime) of particles confined to the energy interval determined by the distribution $n_{\mathrm{F}}(E-\mu_{\mathfrak{L}}(V))-n_{\mathrm{F}}(E-\mu_{\mathfrak{R}}(V))$.

Given the Hamiltonian $\hat{H}$ of the entire system, the calculation of the transmission probability can be delegated to the machinery of the quantum scattering theory. A more practical method represents the system and its parts by Green's functions. To proceed with the latter, it is necessary to partition the Hilbert's space of the system $\mathscr{H}$ into the central region $\mathscr{H}_C$ and left and right reservoirs, $\mathscr{H}_{\mathfrak{L},\mathfrak{R}}$. In Fig. 1.1, the partitioning is illustrated by two dotted lines.

The central region, embedded in the environment (the two leads), is described by the single-particle Green's function (matrix)

$$\mathbf{G}_C(E) = \frac{\mathbf{1}}{E\mathbf{1}-\mathbf{H}_C-\mathbf{\Sigma}_{\mathfrak{L}}(E)-\mathbf{\Sigma}_{\mathfrak{R}}(E)}$$

where $\mathbf{H}_C$ are Hamiltonian matrix elements in the subspace $\mathscr{H}_C$, $\mathbf{1}$ is the unit matrix in $\mathscr{H}_C$. The coupling of the central region to the leads is fully accounted for by the self-energies $\mathbf{\Sigma}_{\mathfrak{L},\mathfrak{R}}(E)$.

With the matrices $\mathbf{\Gamma}_{\mathfrak{L},\mathfrak{R}}(E) \coloneqq \mathrm{i}\Big[\mathbf{\Sigma}_{\mathfrak{L},\mathfrak{R}}(E)-\mathbf{\Sigma}^{\dagger}_{\mathfrak{L},\mathfrak{R}}(E)\Big]$ the transmission function is given by the formula

$$\mathcal{T}(E) = \mathrm{Tr}\Big[\mathbf{\Gamma}_{\mathfrak{L}}(E)\mathbf{G}_C(E)\mathbf{\Gamma}_{\mathfrak{R}}(E)\mathbf{G}_C(E)^{\dagger}\Big] \tag{1.2}$$

given by Caroli, Combescot, Nozières and Saint-James[6].

The virtue of the Green's function approach is twofold: First, it delivers results quickly for few simple, yet descriptive, models (resonant level [1]). Second, the $\mathbf{G}_C(E)$ and $\mathbf{\Sigma}_{\mathfrak{L},\mathfrak{R}}(E)$ can be obtained from an *ab-initio* calculation.

Ab-initio implementation. A long-standing goal of electronic structure theory is to determine single-particle excitation energies and wavefunctions of solids and molecules using only the atomic coordinates and species as input. The so-called *ab-initio* problem requires the solution of the many-electron Schrödinger equation. For a complicated system such as a molecule bound to metallic surfaces the only viable route is density-functional theory (DFT). In particular, it is the Kohn-Sham Hamiltonian that is employed as an effective single-particle Hamiltonian $\hat{H}$ in the transport formalism described above, although this practice does not follow from rigorous DFT. I remark that the *ab-initio* Kohn-Sham states have been used frequently in solid-state physics to gain qualitative insights into the band-structures. Similarly, in quantum chemistry calculations these states provide an often appreciated *molecular-orbital* picture. The calculation of the transmission via Eq. (1.2) parameterized by the Kohn-Sham Hamiltonian has been termed the standard theory of *ab-initio* transport (STAIT) [Article 17]. The review [Article 17] includes a critical discussion of strengths, pitfalls and prospects of improvement of STAIT.

Final remarks address the partitioning that underlies formula (1.2). Naturally, observables should not depend on the way Hilbert's space is partitioned. If $\mathbf{\Sigma}_{\mathfrak{L},\mathfrak{R}}(E)$ were known exactly, $\mathcal{T}(E)$ would indeed be insensitive to the partitioning. In most cases, $\mathbf{\Sigma}_{\mathfrak{L},\mathfrak{R}}(E)$ must be reasonably approximated [7, 8, 9]. The conductance is most sensitive to the atomistic details in the immediate vicinity of the junction. This region provides a 'bottleneck' for the The *ab-initio* calculation of $\mathbf{H}_C$ of a molecular junction typically consists of the molecule plus 50 - 100 atoms of the leads. The details of the electronic structure in regions remote from the junction are actually less relevant. The role of these remote regions in electron transport is to provide charge and momentum relaxation. This motivates a technically simple Ansatz [8, 10], used in the works of this thesis.

Orthogonal basis for partitioning. Hilbert's space partitioning in *ab-initio* calculations requires to construct an orthogonal basis that is local at the same time, since the structure is partitioned in real space. Such basis functions do not belong to the standard equipment of *ab-initio* packages. Often, either the Löwdin orthogonalization procedure or Wannier functions are employed. The author has implemented

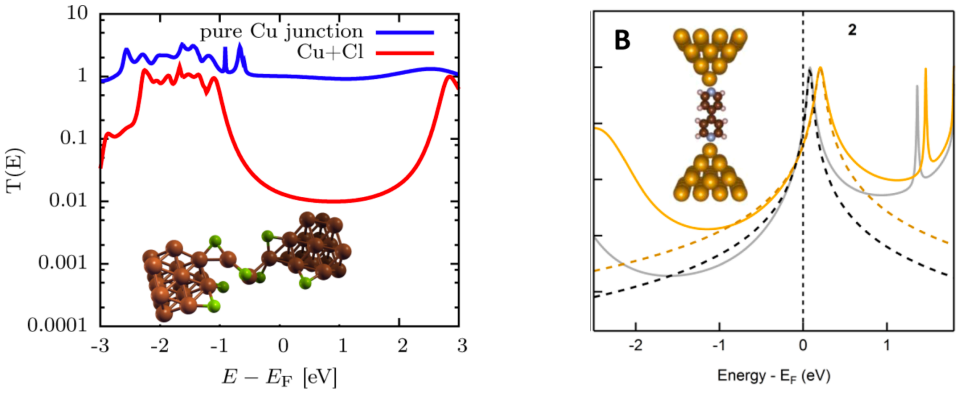

Figure 1.2: First-principles transmission functions. *Left:* atomically-thin copper wire from [Article 7] with Cl adsorbates (inset shows the structure) with adsorbates removed from the junction. Adapted with permission from [Article 7]. Copyright 2014 American Chemical Society. *Right:* 4,4'-bipyridine with Ag (yellow lines) or Au (grey) leads [Article 9]. Dashed lines are Lorentzians fitted to the LUMO peaks. Adapted with permission from [Article 9]. Copyright 2015 American Chemical Society.

an interface that allows to express the Kohn-Sham structure in the Wannier basis in the SIESTA package [Article 16].

TYPICAL TRANSMISSION AND A SINGLE RESONANT LEVEL. The transmission function in the vicinity of the Fermi energy is exemplified in Fig. 1.2 (left) from [Article 7] in the case of a short single-atom thick copper wire. The transmission around E_F approaches 1. The plot also demonstrates the impact of chlorine adsorbates, which drastically reduce the transmission. Such a reduction can not be understood purely from backscattering; in fact, it is caused by conduction electrons being trapped by the electronegative Cl agents. This mechanism is detailed in [Article 7].

For a molecular junction, $\mathcal{T}(E)$ is found to be a collection of resonances which may overlap in energy and often display asymmetric shapes due to quantum interference

[Article 17]. If the energy spacing between resonances is much larger than level broadening, each resonance corresponds to a molecular orbital, as can be easily seen by perturbative arguments. Moreover, $\mathcal{T}(E \approx E_{\mathrm{F}})$ is often determined by a single resonance. Such a resonance must display only tiny asymmetry around its center. This follows from the fact that the scattering phase-shift from neighboring resonances is very close to $\pm\pi$ and is only weakly energy dependent, under the conditions stated above. Under these conditions,

$$\mathcal{T}(E) \approx \frac{4\,\Gamma_{\mathfrak{L}}\Gamma_{\mathfrak{R}}}{(\Gamma_{\mathfrak{L}}+\Gamma_{\mathfrak{R}})^2}\,\frac{1}{1\;+\;\left(\frac{E-E_0}{\Gamma_{\mathfrak{L}}+\Gamma_{\mathfrak{R}}}\right)^2} \tag{1.3}$$

where E_0 is obviously the center of the Lorentzian and the width is given by the broadenings from the left and right leads, $\Gamma_{\mathfrak{L},\mathfrak{R}}$. The prefactor is unity if the latter are equal, in which case we have reflection-free (unitary) transmission for $E = E_0$.

The transmission function from STAIT for 4,4'-bipyridine is shown in Fig. 1.2 (right), along with Lorentzian fits. This result from [Article 9] also demonstrates the impact of the electrode material: the Au and Ag, commonly regarded as similar noble metals. In a collaboration with O. Adak, L. Venkataraman and others, I found that Au-contacted molecules host broader resonances than with Ag contacts. My first-principles calculations revealed that relativistic effects in Au make some fraction of its d-orbitals available for hybridization with the molecule, enhancing broadening of orbital resonances compared to Ag [Article 9].

1.2.2 Anderson impurity model (AIM)

As mentioned earlier, Coulomb interaction in the central region can get effectively strong, because of the localized nature of electronic orbitals and weakened screening. Here I describe a model for a transport scenario beyond CIPA, in which a single orbital in the central region is relevant, only. The only matrix element of the Coulomb interaction retained in this model is the diagonal on-site Hubbard term. The model is known as the Anderson impurity model (AIM). It applies to various other physical contexts (quantum dots, magnetic impurity atoms in alloys, ad-atoms on surfaces). The term 'quantum impurity' is used as an umbrella term for the AIM, its generalizations and relatives.

Description of the AIM

The Hamiltonian of the AIM contains three terms [11]

$$\hat{H} = \hat{H}_1 + \hat{H}_{\text{band}} + \hat{H}_{\text{h}} \,. \tag{1.4}$$

The first term describes the orbital in the central region with on-site energy ε_1 and Coulomb matrix element U,

$$\hat{H}_1 = \sum_{\sigma=\uparrow,\downarrow} \varepsilon_1 \, \hat{n}_{1,\sigma} + U \, \hat{n}_{1,\uparrow} \, \hat{n}_{1,\downarrow} \,, \quad \text{where} \quad \hat{n}_{1,\sigma} \coloneqq \hat{c}^\dagger_{1,\sigma} \hat{c}_{1,\sigma}. \tag{1.5}$$

Here, $\hat{c}_{1,\sigma}$ is the canonical fermionic operator of the electron of spin σ in the impurity (the orbital).

$\hat{H}_{\text{band}}$ is the Hamiltonian of the leads,

$$\hat{H}_{\text{band}} = \sum_{k\sigma} \varepsilon_k \, \hat{n}_{k\sigma} \;, \tag{1.6}$$

where ε_k is the energy of an electron in the lead state k and $\hat{n}_{k\sigma} = \hat{c}^\dagger_{k\sigma} \hat{c}_{k\sigma}$ is the number operator, $\hat{c}_{k\sigma}$ is the annihilation operator of an electron in state $k\sigma$. $\hat{H}_{\text{h}}$ is the Hamiltonian coupling the impurity level and the lead,

$$\hat{H}_{\text{h}} = \sum_{k\sigma} t_k \, \hat{c}^\dagger_{1,\sigma} \hat{c}_{k\sigma} + t_k^* \, \hat{c}^\dagger_{k\sigma} \hat{c}_{1,\sigma} \,. \tag{1.7}$$

The influence of the conduction band on the impurity is entirely contained in the hybridization function

$$\Gamma(E) \coloneqq \pi \sum_k |t_k|^2 \delta(E - \varepsilon_k), \tag{1.8}$$

i.e. the imaginary part of the embedding self-energy.

The AIM has few trivial limits, most notably [12]

Atomic limit is reached when $t_k \to 0$. In the subspace with $N_{\text{d}} = \sum_\sigma \langle \hat{n}_{\text{d},\sigma} \rangle = 1$, the ground state is a spin doublet. The spectrum of charged impurity excitations has two discrete levels at energies $-\varepsilon_{\text{d}}, \varepsilon_{\text{d}} + U$, corresponding to the removal and addition of an electron, respectively.

Resonant level is obtained when $U = 0$ and $|\varepsilon_{\text{d}}| \ll D$. The ground state is a degenerate Fermi gas. In a transport setup with two reservoirs the transmission has the form of Eq. (1.3) under the conditions stated there.

The interesting regime is intermediate between atomic and resonant limits, when $\varepsilon_\mathrm{d} < 0$, $U \approx 2|\varepsilon_\mathrm{d}|$ and $0 < \Gamma \gg U$. Here, the notion of a localized spin doublet interacting with spins of conduction electrons emerges [11]. The notion was formalized by Schrieffer and Wolff [13]. The localized impurity spin is screened by conduction electrons at temperatures below the so called Kondo temperature T_K. The ground state is a spin singlet. Associated with the screening is the appearance of the Kondo resonance in the immediate vicinity of the Fermi level for $T \lesssim T_\mathrm{K}$. An excellent introduction to these concepts can be found in Coleman's book [14].

1.2.3 Extensions of the AIM: Two and more orbitals at work

Quantum transport through molecular junctions and ad-atoms is sometimes not described by a single orbital (in the central region) satisfactorily. In these interesting cases –to be showcased in this thesis– more details of the central region's structure are needed.

Two-impurity model

The two-impurity Anderson model [15] can be seen as an inclusion of a two-valued orbital degree of freedom into the impurity subspace of Eq. (1.4). The interest in this model stems from a rich phase diagram, see [Article 17] for a broader overview. Here, a specific two-impurity Hamiltonian is presented, which can be seen as an Anderson impurity coupled to a spin $\frac{1}{2}$ degree, representing the second impurity. This situation occurs, *e.g.* when the second impurity has charge fluctuations quenched. The dynamics of the first impurity still involves charge fluctuations; in particular, it allows for a current flow in a junction. This special two-impurity Hamiltonian will be called here the 'Double-quantum-dot' (DQD) Hamiltonian.

The impurity part of the DQD Hamiltonian reads

$$\hat{H}_\mathrm{DQD} = \hat{H}_1 + \hat{H}_\mathrm{Z} + \hat{H}_\mathrm{ex}, \tag{1.9a}$$

where $\hat{H}_1$ is identical to (1.5) and

$$\hat{H}_\mathrm{Z} = B\Big(\hat{S}_{z,1} + \hat{S}_{z,2}\Big). \tag{1.9b}$$

$$\hat{H}_\mathrm{ex} = I\,\mathbf{S}_1 \cdot \mathbf{S}_2 \tag{1.9c}$$

The term $\hat{H}_\mathrm{ex}$ represents the exchange interaction between the two electronic degrees of freedom, or impurities. The operators $\mathbf{S}_i$ are the spin projections of the respective

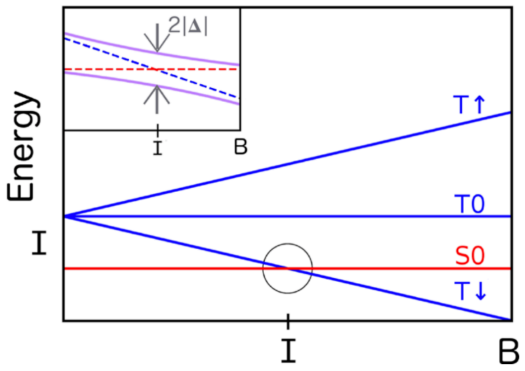

Figure 1.3: Lowest-lying eigen-energies of $\hat{H}_{\mathrm{DQD}}$ as a function of $B > 0$, for $I > 0$. The states are annotated in accordance with Eq. (1.10). The inset is a zoom of the accidental degeneracy point; the degeneracy can be split by magnetic anisotropy terms (not included in $\hat{H}_{\mathrm{DQD}}$), *e.g.* by Eq. (1.11). Purple lines are the resulting avoided crossing. Adapted with permission from [Article 15]. Copyright 2019 American Chemical Society.

impurities. $\mathbf{S}_1$ can be expressed in terms of Pauli matrices $(\sigma_x, \sigma_y, \sigma_z) = \boldsymbol{\sigma}$ as $\mathbf{S}_1 = \frac{1}{2}\sum_{\sigma''\sigma'} \hat{c}^\dagger_{1,\sigma'}\boldsymbol{\sigma}_{\sigma'\sigma''}\hat{c}_{1,\sigma''}$ ($\hbar = 1$). The term $\hat{H}_{\mathrm{Z}}$ represents a homogeneous magnetic field in the z-direction with B in units of energy (Zeeman splitting). With $I = B = 0$ AIM is recovered.

In the subspace with $\sum_\sigma \langle \hat{n}_{1,\sigma}\rangle = 1$, the lowest-lying eigenstates of $\hat{H}_{\mathrm{DQD}}$ are spin-triplet (T) and singlet (S) states, split by the Zeeman field,

$$|S0\rangle = \frac{1}{\sqrt{2}}(|\uparrow\downarrow\rangle - |\downarrow\uparrow\rangle), \qquad E_{S0} = \varepsilon_1 - \frac{3I}{4} \tag{1.10a}$$

$$|T\uparrow\rangle = |\uparrow\uparrow\rangle, \qquad E_{T\uparrow} = \varepsilon_1 + B + \frac{I}{4} \tag{1.10b}$$

$$|T0\rangle = \frac{1}{\sqrt{2}}(|\uparrow\downarrow\rangle + |\downarrow\uparrow\rangle), \qquad E_{T0} = \varepsilon_1 + \frac{I}{4} \tag{1.10c}$$

$$|T\downarrow\rangle = |\downarrow\downarrow\rangle, \qquad E_{T\downarrow} = \varepsilon_1 - B + \frac{I}{4}, \tag{1.10d}$$

where in the symbol $|\uparrow\downarrow\rangle$ the first (second) arrow represents the spin projection of the first (second) dot, respectively. The spectrum of $\hat{H}_{\mathrm{DQD}}$ is shown in Fig. 1.3. At $B = 0$ the ground state is either the singlet ($I > 0$) or the triplet (the $I < 0$ is ferromagnetic). Finite B splits the triplet, causing an accidental degeneracy at $|B| = |I|$.

The coupling to the leads is introduced to this model by adding $\hat{H}_{\rm band} + \hat{H}_{\rm h}$ from Eqs. 1.6,1.7 to $\hat{H}_{\rm DQD}$. At the accidental degeneracy point, Kondo effect, involving fluctuations of the singlet and 1 triplet component, was predicted [16, 17].

Anisotropic exchange. In presence of spin-orbit coupling, spin is no longer conserved. Consequently, the exchange $\hat{H}_{\rm ex}$ and the Zeeman term $\hat{H}_{\rm Z}$ adopt an anisotropic form with effective g and I tensors [18]. I assume here that such anisotropies are the smallest energy scales in the Hamiltonian, which is true in most materials free from heavy elements.

Of interest is the action of these anisotropies on the accidental degeneracy. A trivial consequence can be the shift of the degeneracy point. A more interesting one is gap opening by an avoided crossing, which will be explored in Sec. 3.3.2. It turns out that the degeneracy is lifted, quite generically, by the anti-symmetric exchange terms of the form

$$H_{\rm A} = -2\sqrt{2}\,\Delta\,\Big(\,\hat{S}_1^x\,\hat{S}_2^z\,-\,\hat{S}_1^z\,\hat{S}_2^x\,\Big), \tag{1.11}$$

called the Dzyaloshinskii-Moriya interaction. The $2|\Delta|$ is the singlet-triplet gap at $B = I$ (see inset of Fig. 1.3).

Multi-impurity Anderson model

Previously, I have shown an extension of the AIM to two impurities, that interacted strongly by exchange [Eq. (1.9)]. Here, I consider the case of a negligible inter-impurity exchange, applicable to impurity orbitals that can be thought as well-separate from each other. The multi-impurity Anderson Hamiltonian reads,

$$\hat{H} = \sum_{k\sigma} \epsilon_k \hat{c}^\dagger_{k\sigma}\hat{c}_{k\sigma} + \epsilon_{\rm d}\sum_{m\sigma}\hat{d}^\dagger_{m\sigma}\hat{d}_{m\sigma} + U\sum_m \hat{d}^\dagger_{m\uparrow}\hat{d}_{m\uparrow}\hat{d}^\dagger_{m\downarrow}\hat{d}_{m\downarrow} + \\ + \sum_{k\sigma}\sum_m\Big(V_{km}\hat{c}^\dagger_{k\sigma}\hat{d}_{m\sigma} + \text{ h.c.}\Big), \tag{1.12}$$

where the first term has the usual meaning (see (1.6)), the second term stands for M impurities ($m = 1, \ldots, M$) with equal on-site energies $\epsilon_{\rm d}$, the third term is a Hubbard-type repulsion on each impurity orbital and the last term is a multi-impurity extension of the hybridization term (1.7). The Hamiltonian (1.12) has been used to describe chains of magnetic ad-atoms on a metallic surface [Article 14].

It is well known that the model Eq. (1.12) describes a conduction-band mediated exchange mechanism called the RKKY exchange [18]. A regime in which the corresponding exchange energy lies below the Kondo scale is of interest (see Results). The cross-talk between impurities remains, but it is of single-particle nature; *i.e.* it is a substrate-induced hybridization. Mathematically, it originates as follows. The effect of the substrate on the impurities is fully represented by the embedding self-energy $\Sigma_{ij}(\omega)$. It is an ω-dependent $M \times M$ matrix in the impurity orbital space. The real part of the diagonal terms Σ_{ii} shifts the impurity levels; the imaginary part broadens them. The off-diagonal terms henceforth represent substrate-mediated hybridization (non-Hermitian and retarded). Due to analyticity, it suffices to know the anti-Hermitian part of the embedding self-energy, called the *hybridization function* $\Gamma_{ij}(\omega) \coloneqq \frac{\mathrm{i}}{2\pi}\Big[\Sigma_{ij}(\omega) - \Sigma^*_{ji}(\omega)\Big]$.

It is both instrumental and instructive to evaluate $\Gamma_{ij}(\omega)$ for a homogeneous electron gas with point-like impurities sitting on a line with spacing d,

$$\Gamma_{ij}(\omega) = \Gamma_0 \; J_0(kd|i-j|) \cdot \Theta(E_0^2 - \omega^2) \qquad D = 2 \text{ dimensions} \tag{1.13}$$

$$\Gamma_{ij}(\omega) = \Gamma_0 \; \frac{\sin(kd|i-j|)}{kd|i-j|} \cdot \Theta(E_0^2 - \omega^2) \qquad D = 3 \text{ dimensions.} \tag{1.14}$$

In the above expressions, k is defined by inverting inverting the dispersion $\epsilon_k \equiv \omega$. $2E_0$ is the band-width and Γ_0 is the single-impurity hybridization function [see Eq. (1.8)] [Article 14]. Due to translational invariance of the substrate, the expressions depend on the impurity distance $R_{ij} \coloneqq |i-j|d$ only. Notice, that the hybridization has a long-range character: Along the chain it decays as $R_{ij}^{-(D-1)/2}$. For states at the Fermi level, the off-diagonal part of $\Gamma_{ij}(E_\mathrm{F})$ oscillates in sign as a function of R_{ij}.

Local density of states. Many-body techniques targeted at the impurity models usually deliver the retarded Green's function of the impurity subspace, $G_{ij}(\omega)$. The Green's function of the substrate, $\mathcal{G}(\mathbf{r}, \mathbf{r}'; \omega)$, is given by the expression [19]

$$\mathcal{G}(\mathbf{r}, \mathbf{r}'; \omega) = \mathcal{G}^{(0)}(\mathbf{r} - \mathbf{r}';\ \omega) + \gamma \sum_{ij} \mathcal{G}^{(0)}(\mathbf{r} - \mathbf{R}_i;\ \omega) G_{ij}(\omega) \mathcal{G}^{(0)}(\mathbf{R}_j - \mathbf{r}';\ \omega), \tag{1.15}$$

where the Green's function of the unperturbed substrate (free from impurities) is decorated with a superscript (0) and $\gamma \propto \Gamma_0$. The Eq. (1.15) is a consequence of the block-matrix structure of the Anderson models, plus two additional simplifications: (1) the impurities are assumed to be point-like, located at positions $\mathbf{R}_i$; (2) the

substrate is homogeneous. The Eq. (1.15) can serve to predict scanning-tunneling spectra: The local density of states is simply $\rho_s(\mathbf{r},\omega) = -\mathrm{Im}\mathcal{G}(\mathbf{r},\mathbf{r},\omega)/\pi$.

2 Quantum size-effects in molecular junctions

One of the first achievements of early quantum theory was the explanation of stability and optical properties of free atoms. Soon after that, the discovery of electron bands and spontaneously-broken phenomena (magnetism, superconductivity, *etc.*) in solids brought macroscopic quantum behavior to the forefront [20]. Natural question arose: How does the macroscopic emerge when we start assembling the atoms together?

For theorists, these questions became very tangible with the advent of the nanoscale era, where collecting atoms and molecules into arrays became possible. Most of this chapter concerns with size effects from fusing together few pieces of a basic building block, *e.g.*, an atom or molecular substructure. An exception is the following section, where size effects result from the compression of a molecular junction.

2.1 Size-effects from molecular junction compression

One of the biggest advantages of molecular-junction setups is the built-in possibility to stretch or pull the molecular bridge. If the transport is dominated by a single frontier orbital (resonance), it is possible to investigate the effect of the junction compression on the resonance. A remarkable example occurs in the weakly-coupled limit: The electrostatic energy of an electron transferred to the molecule has a contribution from image charges in the electrodes. Junction stretching reduces the image-charge energy, resulting in shifts of the resonance energy. This physical picture was invoked by Perrin *et al.* [21] for thiolated porphyrin molecules contacted by gold. Perrin *et al.* termed this effect *mechanical gating*. Let me point out that for the above picture to apply, the molecular orbital must be well separated from the

electrodes. This happens in many molecular junctions in which a molecule attaches to the electrodes via chemical linker groups ('thiolation' in the above case).

In collaboration with J. Šebesta, B. Pabi, O. Tal and A. Pal we found a molecular junction with strong mechanical gating, yet operating differently than the mechanism described above. The ferrocene molecule is rather small and its frontier orbitals hybridize directly with the Ag electrodes without linker groups [Article 22]. Consequently, electron lifetimes are much shorter. But because of direct coupling without linkers, the wavefunction of the frontier orbital penetrates to the leads. The image-charge mechanism (utilizing point charges) must be considerably weakened. In STAIT calculations found evidence for mechanical gating without invoking image charges. The electrostatic shifts in ferrocene/Ag levels result from reorganization of charge density –in the molecule– upon junction stretching. The reorganization can be roughly seen as having two major sources: penetration of the surface density into the molecule and redistribution of charge density in electrode-molecule bonds.

2.2 Qualitative understanding of length-scaling of excitation gaps and conductances of oligomers

Consider an oligomer – a molecule with a unit cell repeated N times linearly (see Fig. 2.1(a) for an example). Of interest here will be the length dependence of the lowest excitation gap, $\Delta_g(N)$, of the oligomer in isolation. Then, a discussion of the conductance of the molecule coupled to leads follows.

2.2.1 Scaling of the excitation gaps

The behavior of $\Delta_g(N)$ results from two factors that need to be considered: band-structure and interaction effects, to be discussed in the following.

The role of band-structure. For weakly correlated systems, electron-electron interaction is accounted for in the effective single-particle Hamiltonian in a mean-field-like fashion. The lowest excitation gap is the difference in single-particle energies of the lowest unoccupied molecular orbital (LUMO), and the highest occupied molecular orbital (HOMO). Namely, $\Delta_g := \epsilon_{\mathrm{LUMO}} - \epsilon_{\mathrm{HOMO}}$. To understand its N-dependence, the spectrum of an infinitely long specimen is of interest (band-

structure). The band-structure is either metallic or insulating. For an oligomer of the metallic kind (molecular wire)

$$\lim_{N\to\infty} N\Delta_{\mathrm{g}}(N) = 0 \tag{2.1}$$

must hold.

In metallic quasi-1D systems with a single band intersecting E_{F} the simple behavior

$$\Delta_{\mathrm{g}}(N) = \frac{A_1}{N} + \frac{A_2}{N^2} + \mathcal{O}\big(N^{-3}\big) \tag{2.2}$$

is observed. The coefficients A_1 and A_2 can be given a band-theoretic interpretation. Let's assume the infinite oligomer (polymer) has a single band intersecting the Fermi level. The orbital energies of finite oligomers are obtained by quantizing the wavenumber k; the number of allowed k's increases proportionally with N. It can be anticipated, that A_1 is proportional to the Fermi velocity and the band curvature enters A_2. As I will show in Sec. 2.3, the $\Delta_{\mathrm{g}}(N)$ is more interesting when there are two partially-filled bands.

Gaps of oligomers that have an insulating band-structure follow the law

$$\Delta_{\mathrm{g}}(N) = \Delta_{\mathrm{g}}(\infty) + \frac{A}{N} + \mathcal{O}\big(N^{-2}\big)$$

with the band gap $\Delta_{\mathrm{g}}(\infty)$.

Interaction effects. Unscreened Coulomb repulsion changes the leading N^{-1} power law in $\Delta_{\mathrm{g}}(N)$ in Eq. (2.2). To be specific, let $\Delta_{\mathrm{g}}(N)$ denote the so called fundamental gap, defined by

$$\Delta_{\mathrm{g}}(N) \coloneqq E_{N_{\mathrm{e}}+1} - E_{N_{\mathrm{e}}} - E_{N_{\mathrm{e}}} + E_{N_{\mathrm{e}}-1},$$

where the respective terms are ground-state energies of the system (molecule, cluster) with given number of electrons; N_{e} is the neutral-state electron number. The fundamental gap thus equals the difference in energies required to add/remove an electron from the neutral state, aka the difference in ionization potential and electron affinity. At a mean-field level of the theory, the fundamental gap can be thought as having two components: the difference in molecular orbital energies (the HOMO-

LUMO gap) and the electrostatic charging energy. The scaling of the charging energy follows from the Coulomb repulsion integral

$$U := \frac{e^2}{2} \int \mathrm{d}^3\mathbf{r}\, \mathrm{d}^3\mathbf{r}'\, \frac{\varrho(\mathbf{r})\varrho(\mathbf{r}')}{|\mathbf{r}-\mathbf{r}'|} \tag{2.3}$$

where $\varrho(\mathbf{r})$ is the density of a frontier orbital, normalized to unity. Assuming that the frontier orbitals (HOMO, LUMO) are distributed homogeneously over the system, the integral scales as $U \propto V^{-1/3}$ with volume V. The scaling resulting from the integral (2.3) follows essentially from dimensional arguments, *i.e.* it is not shape dependent. For oligomers it suggests that interaction effects will tend to slow down the N^{-1} power law.

Gaps of metallic grains

The previously presented ideas from this section have a side-application that I discuss here. Consider metallic disordered clusters (amorphous grains). Such grains often model electrodes in quantum transport. An ordered metallic system has a conduction band with a finite bandwidth W. A moderately weak disorder that preserves locality will not alter W significantly for all grain volumes V. Since disorder induces level repulsion, the average excitation gap must scale as $\propto W/V$, if we exclude interaction effects. Thus, the gap of the grain decreases as $1/N$ with the number of atoms, as in Eq. (2.2). Interaction effects will alter the N^{-1} power law to $N^{-1/3}$, as anticipated from Eq. (2.3).

In [Article 25] we employed the post-DFT GW approximation to calculate the charged excitations of disordered metallic grains. We found the $N^{-1/3}$ scaling of the HOMO/LUMO gaps and a $1/N$ scaling of gaps of occupied states. Thus, the widened HOMO/LUMO gap results in a depleted density of states around the E_F when such grains are employed as electrodes for quantum transport. The GW approximation will likely not deliver a quantitative improvement, when used in STAIT instead of DFT.

2.2.2 Conductance of molecular wires as a function of length

Let me denote the length dependence of the conductance of molecular wires (oligomers) by $G(N)$. This observable played a pivotal role in early molecular electronics because it allowed to benchmark computational techniques [Article 17]. Here I give a qualitative discussion.

In the CIPA, the length dependence of the linear conductance is the length dependence of $\frac{2e^2}{h}\mathcal{T}(E_\mathrm{F})$. For a single resonant level, Eq. 1.3, coupled symmetrically, $\Gamma_\mathfrak{L} = \Gamma_\mathfrak{R} \coloneqq \Gamma$, the $G(N)$ is given by the length dependencies $\Gamma(N)$ and $E_0(N)$.

In molecular wires (oligomers), the frontier orbitals are delocalized across the molecule. The lifetime of an electron put to such an orbital will be proportional to N, therefore,

$$\Gamma(N) = \frac{c}{N} + \mathcal{O}\big(N^{-2}\big). \tag{2.4}$$

Metallic wires. For metallic wires, the $E_0(N)$ must approach the Fermi level at $N \to \infty$, due to the HOMO-LUMO gap closing:

$$E_0(N) \approx E_\mathrm{F} + \frac{\epsilon_1}{N} + \frac{\epsilon_2}{N^2} + \dots \tag{2.5}$$

Using the Eqs. (2.5, 2.4, 1.3) it is easy to find the scaling of the conductance [Article 10],

$$G(N) \approx \frac{G(\infty)}{1 + 2\frac{\epsilon_1}{\epsilon_2}N_c^2/N + (N_c/N)^2}, \tag{2.6}$$

where N_c and $G(\infty)$ depend on c and $\epsilon_{1,2}$, only. When $\epsilon_{1,2}$ have equal signs, the conductance increases monotonously, approaching the limit $G(\infty)$ from below. With unequal signs, $G(N)$ can be non-monotonous. See [Article 17] for an application of these scaling arguments to the measured conductances of Oac with linker groups in [22]. The discussion of Oac free from linker groups is presented in Sec. 2.4.

Insulating wires (remark). For the sake of comparison with the previous scenario, I mention insulating wires, also because of their importance in the early molecular electronics [23, Article 17]. The most commonly used molecules involved thiol linkers. Consequently, these molecules are much less coupled to the metals and the transport is considerably off-resonant, rendering the Lorentzian formula (1.3) inapplicable. For N large enough that HOMO and LUMO energies become constant, the length dependence of the conductance follows from semi-classical tunneling arguments,

$$G(N) = G_0 e^{-\beta N}.$$

In the work [Article 11] we investigated (in a theory-experiment collaboration) molecules with strong spin-orbit coupling (containing Si) with Au leads. The STAIT calculations (in collaboration with V.Pokorný and María Camarasa) showed an exponential decay of $G(N)$, validating the tunneling picture.

2.3 Quantum size-oscillations of oligoacene excitation gaps

Oligoacenes (Oac) are text-book examples of oligomers, molecules that are composed of a repeating unit cell. The smallest one is benzene and it has one hexagonal carbon ring (Fig. 2.1). Further Oac can be 'built' by amalgamating rings linearly. One could perceive oligoacenes as a limiting case of a narrow graphene nanoribbon, although very little from the graphene's electronic properties is left.

2.3.1 Incommensurate gap oscillations

The nature and spectrum of excitations in Oac has been subject to an intense debate. The infinitely long Oac is gapless within independent-particle approaches, $\Delta_g(\infty) = 0$, and it was suggested to host unconventional superconducting pairing [24]. For quantum chemistry, the Oac are very rewarding molecules, because their gas-phase properties reflect strong correlation [25, 26]. The lowest excitation gap, $\Delta_g(N)$, as a function of the number of rings N, is very suited to study the interplay of electron-electron interaction and band-structure effects.

In 2014 I and my coworkers proposed that band-structure effects should have a remarkable imprint on $\Delta_g(N)$ [Article 6]. The effectively-independent electron approaches (DFT, tight-binding) actually predict an oscillatory $\Delta_g(N)$; only the amplitude of the oscillations decays as $1/N$, see Fig. 2.1. At regular intervals the gap vanishes. The amplitude of the oscillations, ≈ 11, is incommensurable with parameters of the lattice. The oscillations of $\Delta_g(N)$ are a reflection of the band-structure of an infinitely long Oac. They are caused by two bands crossing each other at the Fermi level.

My 2014 work has the following implications were suggested: First, even with strong interaction effects dominated the $\Delta_g(N)$ behavior, the oscillations could still superimpose. Second, and more important, when Oac are in contact with screening environments, such as liquids and metallic surfaces, the interaction effects are weaker.

Therefore, two theoretical questions followed:

1. How is the electronic structure of Oac changed by the adsorption to the Au surface?

2. What is the gap behavior when we combine the band-structure effects with local (screened) Coulomb repulsion?

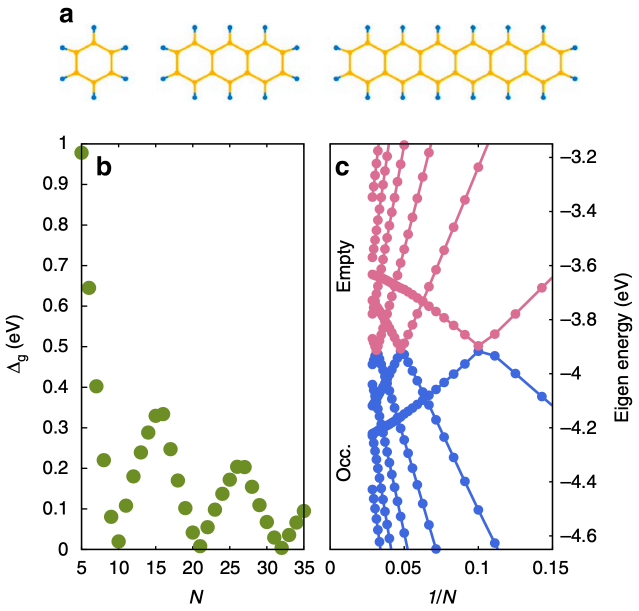

Figure 2.1: (a) Examples of oligoacenes with N rings: benzene ($N = 1$), anthracene ($N = 3$) and hexacene ($N = 6$); carbon (hydrogen) atoms are yellow (blue) dots. (b) Dependence of the HOMO-LUMO gap on N, showing a non-monotonous behavior with incommensurate oscillations. (c) Kohn-Sham spectrum, showing occupied (blue) and unoccupied (pink) states. Near $N = 10, 21, \ldots$ there is a crossing of HOMO and LUMO. Reproduced from [Article 6] with permission.

I addressed the former in a collaboration with M. van Setten, D. Xenioti *et al.* [Article 13] in the framework of density functional theory. The on-surface Oac excitation gap $\Delta_g(N)$ was calculated for molecules until $N = 7$. The extrapolation lo larger N clearly gap closing for $N \approx 11$, suggesting, that the oscillations remain present on Au, if correlation effects remain weak.

I addressed the second question using an Oac tight-binding lattice model with an on-site Hubbard repulsion [Article 12]. In a team with P. Schmitteckert and others we employed density-matrix renormalization group to obtain a numerically-exact excitation spectrum. We found that the oscillations are surprisingly robust even if the Hubbard term U approaches the width of the carbon π bands.

2.3.2 Comparison with the experiments

The previous review of my theoretical contributions to the field in the years 2014-2019 would be incomplete without mentioning the experimental results from this quickly developing field. Right graph of Figure 2.2 shows the length dependence

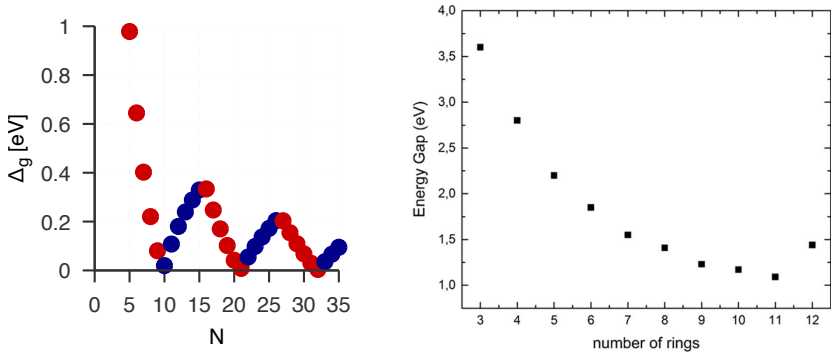

Figure 2.2: Length dependence of the lowest excitation gap of Oac. *Left:* Theoretical Kohn-Sham HOMO-LUMO gap [Article 6], reproduced with permission. *Right:* Experimental scanning-tunneling gap [27] defined as the energy difference of the two resonances in the differential conductance, immediately above and below the Fermi energy. Reprinted with permission from [27]. Copyright 2020 American Chemical Society.

of the transport gap of Oac on Au measured by STM and reported by Eisenhut *et al.* [27] and Krüger *et al.* [28]. A minimum is visible for $N = 11$, followed by an upturn. The trend until $N = 11$ was already analyzed by me and coworkers [Article 13] and seen consistent with band-structure arguments. The more recent synthesis of dodecacene ($N = 12$) [27] showing the upturn is even more suggestive. The reader has certainly observed that the experimental trend has an offset ≈ 1 eV with regards to the theoretical KS-DFT (effectively non-interacting) gap. This offset can be interpreted as the charging energy, preventing the gap to fully close. As I detail below, it is not clear whether the upturn has to do with band-structure effects.

Open questions and controversies. A theoretical consensus about the Oac-on-Au gap scaling is still lacking. On one hand, quantum-chemical calculations point to strong correlation effects, termed *polyradical* [25]. On the other hand, in the weakly correlated limit (when interaction is screened), band-structure arguments should apply.

Eisenhut *et al.* criticized the band-structure arguments because the latter presumably lack polyradical behavior discussed for gas-phase specimen [27]. This argument is obviously not straightforwardly applicable to the Au surface due to screening. Ruan and coworkers [29] discuss the band-structure effects, admitting that the effect of the surface on the strong molecular electron-electron interaction is not un-

derstood. The authors prefer an interpretation based on spin-polarized DFT, which is also consistent with the measured gap. In the latter, the polyradical phenomenon manifests as a molecular magnetization. It is possible to formulate a critique to the use of spin-polarized DFT: It is known in electronic structure theory that 'magnetized' solutions hint towards strong interaction effects, but they do not describe excitations properly [30]. This so called Löwdin symmetry dilemma is known since the earliest restricted and unrestricted Hartree-Fock calculations.

From band theory it follows that the first gap minimum ($N \approx 11$) is accompanied by a change in the symmetry of HOMO: from odd to even with respect to a mirror plane that bisects the Oac into two wires. In STM this transition should manifest as a disappearance of a nodal plane in the HOMO resonance. This has not been observed. Ruan *et al.* reported presence of such a plane for $N = 13$. This would go against the oscillatory band arguments. As a matter of fact, in 2024 two groups reported inconsistent gap sizes for $N = 13$: 1.40 eV [31] and 1.09 eV [29]. Evidently, the STM approach to the measurement of the fundamental gap requires further scrutiny. The trend of the gap of these molecules remains to be of vivid interest and fundamental importance.

2.4 Metallicity in oligoacene molecular wires

In a collaboration with O. Tal, T. Yelin, and others, we explored the conductances of oligoacene molecular junctions with N up to 6 [Article 10].

When the Oac are attached to Ag electrodes, the level broadening Γ is much smaller than the level spacing. My transmissions, Fig. 2.3, demonstrate that the transport is governed by the LUMO resonance. The gap oscillations do not need to be considered because the molecules are short. The measured average $G(N)$ shows an increase and a saturation around $0.6G_0$, consistent with the formula (2.6) [when $\epsilon_1\epsilon_2 > 0$]. The 'anti-Ohmic' trend nicely exemplifies quantum-coherent transport behavior.

On the contrary, the Oac contacted by platinum electrodes have level spacing of the same order as the level broadening, Γ. This is because platinum has a partially-filled d-band and therefore more states are available to hybridize with Oac compared to silver, as I elucidated in the [Article 4]. In this regime of strong molecule-electrode hybridization, $\mathcal{T}(E)$ weakly varies around unity and is free from deep drops, as my STAIT calculations showed [Article 4]. This is consistent with the experimental average conductance $G(N)$, observed constant, within the statistical error bar.

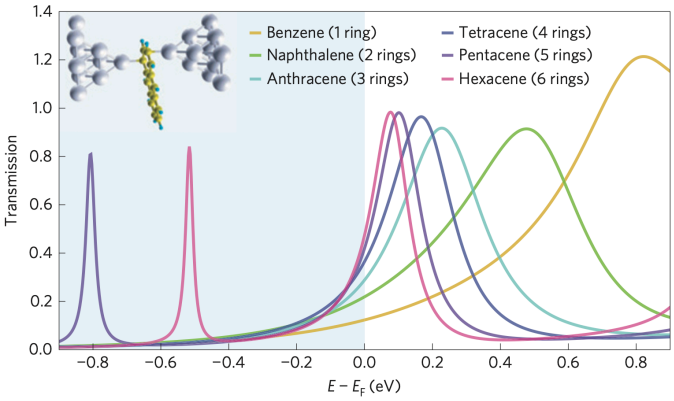

Figure 2.3: Transmission functions of Oac coupled to Ag electrodes from first-principles DFT calculations. Conductance, $2e^2\mathcal{T}(E_\mathrm{F})/h$, is increasing with the number of rings, in stark contrast with Ohm's law. Reproduced from [Article 10] with permission.

Side-note: magnetic instability in Pt. When exchanging Ag tips for Pt, one needs to pay attention to one subtlety. Platinum is non-magnetic in bulk, but under-coordination causes local magnetic ordering in nanowires and chains [32]. I have shown, along with F. Evers, that local ordering also happens at the apex of a Pt tip [Article 3]. Such magnetic ordering has been observed experimentally in single-atom Pt point contacts [33]. The impact of magnetism on the conductance of short Pt chains is approximately 20% [34], and the tendency to order is weaker when there is a molecular bridge, due to improved coordination. Therefore, the eventual magnetism is not essential to understand transport through Oac.

3 Strong electronic correlation in molecular and atomic adsorbates

The progress in the fabrication of nanoscale systems in recent decades brought a resurrection of the Kondo problem and an associated outburst of theoretical works. My works presented in this thesis focus on the Kondo behavior in magnetic ad-atoms on surfaces and magnetic molecules. This chapter starts with a quick overview of molecular/ad-atom Kondo behavior and follows with sections with increasing complexity of the 'impurity' subspace. First, systems that can be understood in a 'single-impurity' framework are presented. Second, molecular adsorbates with two coupled spin degrees of freedom follow. Finally, a system of a 'multi-impurity' character is shown.

3.1 A brief overview of nanoscale Kondo phenomena

Here I offer a broader perspective on the field of Kondo behavior at nanoscale. By nanoscale I refer to single magnetic atoms, molecules, but also carbon nanotubes and quantum dots. These constituents take place of the 'impurity' in impurity models. What has this theoretical and experimental development brought?

(i) The nanoscale Kondo systems usually contain a single 'impurity' that is being addressed, *e.g.* by some form of spectroscopy. In contrast, in the alloy systems, where Kondo behavior was first discussed, single-impurity behavior undergoes ensemble averaging.

(ii) The main source of observables is electronic transport at finite bias. This gives access to excitations at finite energy (from the Fermi level) and non-equilibrium effects.

(iii) The previous two factors pave way to observing more intricate internal structure of the Kondo impurity. The simplest spin-$\frac{1}{2}$ Kondo Hamiltonian often

needs to be extended to capture spin multiplets (in ad-atoms) and molecular orbital structure (in molecular adsorbates). The transport spectroscopy in such systems can host Kondo peaks with nontrivial shapes, with satellite peaks, offering a view of the internal electronic structure of the atom or molecule.

(iv) In molecules the situation is arguably the most complex. Apart from the electronic spin and orbital low-energy structure, molecules also host low-energy vibrational excitations, which manifest as side-peaks.

(v) Ad-atoms and molecules on surfaces can be locally manipulated by the STM tip. Moreover, it is possible to design multi-impurity structures, such as corrals, arrays, chains, etc., offering a new possibility to address the collective correlated behavior of lattice models (*e.g.* Kondo lattice).

A more detailed overview with references can be found in the co-authored review [Article 17] (with emphasis to molecular systems).

3.2 Single-impurity molecular Kondo systems

3.2.1 Inelastic transitions in a Kondo impurity

An excited state of an adsorbate (atom, molecule) can decorate the STM transport spectrum ($\mathrm{d}I/\mathrm{d}V$ vs. voltage V) with step-like features, if transition matrix elements are non-zero [35, 36]. In the language of scattering theory, such transitions are inelastic, because the adsorbate is left in an excited state after the passage of the tunneling electron. In contrast, the usual quasiparticle excitations of adsorbates (*i.e.* effective single-particle physics) are energy-conserving and therefore, elastic.

Inelastic spin transitions

Consider a molecule with a singlet ground-state and a triplet of excited states, attached to two leads (transport setup). The Hamiltonian (1.9) is applicable. Furthermore, the second lead couples infinitesimally weakly (it acts as a probe), and does not need to be included – the differential conductance is proportional to the impurity spectral function in this limit.

My work [Article 1] provided a calculation and analysis of the spectral function, with emphasis on the inelastic transitions (near energy $E - E_\mathrm{F} \sim |I|$ for $B = 0$). From the scattering-theoretic viewpoint, the inelastic scattering off the

singlet-triplet molecule involves multiple 'collisions', which rules out a simple Born-type approach. Moreover, Kondo scattering requires the theoretical machinery to account for the Fermi sea (many electrons obeying Pauli principle). I employed all-orders many-body perturbation theory for this purpose. With Jean-Pierre Gauyacq and Nicolás Lorente we compared the results from the many-body theory with a sudden-approximation approach (no Kondo scattering). This allowed us to estimate the renormalization of the inelastic threshold and other quantities relevant for the scanning-tunneling spectroscopy.

Inelastic vibrational transitions

Molecular vibrational excitations can be detected in electron transport as side-bands (in the $\mathrm{d}I/\mathrm{d}V$), similarly to the previously mentioned spin excitations. Additionally, when the adsorbed molecule hosts a Kondo resonance, the vibrational side-bands morph into side-peaks of the zero-bias Kondo peak. With my collaborators (at Weizman Institute) I contributed to establish this picture in a theory – experiment collaboration [Article 5]. The side-peaks were observed in a silver break-junction with copper phthalocyanine (CuPc). My DFT calculations established that CuPc attached to Ag electrodes has to be treated a spin-half doublet. This came as a surprise in view of the more intricate spin-orbital structure of CuPc adsorbed flat on Ag(111) [37, 38]. The spin-half multiplicity of CuPc in a break-junction was a first indication, that the measured side-peaks are not spin but vibrational excitations. Calculations of vibrational excitations of CuPc in a junction helped to identify a particular mode whose energy and stretching dependence matched with the experimental.

This work demonstrates that DFT calculations, when interpreted correctly, can be very helpful for explaining a physical setup that involves strong electronic correlations. Of course, DFT with semi-local correlations do not capture Kondo-type correlations. Therefore, the results of such calculations can not be taken literally. However, the atomistic DFT calculations can be very instrumental in identifying the relevant degrees of freedom and choosing the right phenomenological model.

3.2.2 Kondo temperature

A simple spin-half Kondo impurity can be associated with various local observables, such as conductance, spectral function or magnetic susceptibility. Their temperature dependencies carry an imprint of the cross-over between a local-moment regime

('weak coupling') and Fermi-liquid 'strong-coupling' regime [19]. Because it is a cross-over, the transition temperature (Kondo temperature T_K) is not sharply defined. Intricately, in a spin-half molecular junction, the differential conductance hosts a zero-bias peak in both regimes. Since temperature can not be easily changed over few orders of magnitude in an experiment, the following question arises: Observing a zero-bias peak in a molecular junction at a fixed temperature T, how can one identify whether the junction is in a weak or strong-coupling regime? Even more ambitiously: Can one estimate the ratio T/T_K?

It turns out that T_K can be determined rigorously even if T can not be changed, but when magnetic field is available instead [Article 18]. A convenient experimental setup is a junction, whose T_K can be tuned mechanically by junction stretching (measurements of P. Jelínek, M. Švec (FZÚ AVČR) and coworkers). Their results were fitted by spectral functions from a numerical-renormalization group calculations (M. Žonda, MFF Charles University). In this collaborative work I identified a voltage-asymmetric vibrational peak, whose behavior could be consistently explained by the trend in the source-drain asymmetry.

Magnetic molecules with zero Kondo temperature

Adsorbed magnetic molecules with a vanishingly small Kondo temperature are of special interest, too. Conceptually, there are two ways to achieve $T_K = 0$ in a Kondo impurity:

(i) The fermionic reservoir (substrate) has a gap E_g at E_F. The ground-state is a doublet when E_g is large enough [39]. If such a system is realized in a molecular adsorbate, it can represent a local qubit.

(ii) The impurity's ground-state spin multiplet is split by spin-orbit coupling (magnetic anisotropy splitting). If the anisotropy prefers a large spin, Kondo screening can be quenched [40]. Such molecular adsorbates are single-molecule magnets (SMM); they retain their functionality even when contacted by metallic electrodes provided that the interaction with the metal is not too strong to bring Kondo screening into play.

Reference [Article 20] shows an example of a SMM adsorbed on a transition-metal dichalcogenide. My DFT calculations showed that the molecule-substrate interaction is very weak and the SMM behavior is preserved.

3.3 Two-impurity Kondo systems realized as molecules

Materials that contain atoms which retain their magnetic moments even in presence of a metallic band can host intricate behavior [14]. These strongly-correlated systems are often difficult to treat theoretically even with relatively basic models, such as a Kondo or Anderson lattice. Certain aspects of these lattice systems can be explored in a somewhat easier way in so called two-impurity Kondo systems. In recent years, molecules (as adsorbates and junctions) have been used in experiments to target the two-impurity physics, which in turn stimulated additional theoretical progress. I refer the reader to the review [Article 17] for the list of few important works, and follow with author's selected works.

3.3.1 Bi-nuclear magnetic molecule

An extensive theoretical and experimental investigation of bi-nuclear complexes was undergone at KIT (Karlsruhe) by me, A. Bagrets, W. Wulfhekel, F. Evers, L. Zhang and others. These complicated molecules contain two transition-metal centers, which were separated by a bi-pyrimidine ligand, bridging the two centers. The centers were Ni, Mn and Zn. An analysis assisted with DFT calculations lead us to conclude that the Ni_2 complex on Cu(100) is a double spin-one Kondo impurity. Each Ni center (impurity) undergoes partial Kondo screening independent from the other, because the cross-talk (precisely, exchange interaction) between the two centers is very weak [Article 8].

3.3.2 Dzyaloshinskii-Moriya interaction in a diradical

While in the previous example, the two molecular magnetic moments (impurities) didn't interact, the opposite case of a strong exchange is of interest, too. When spin-orbit effects are weak, the isolated molecule with two spin-half centers has the low-energy spectrum given by Eq. (1.10).

With P. Zalom and T. Novotný (Charles University) we employed numerical renormalization group to investigate the DQD model [Eqs. (1.9) and (1.11)] near the singlet-triplet crossing. We found, surprisingly, that despite the terminology 'Kondo screening', spin polarization persists in the reservoir. Clearly, this is a consequence of the fact that the local spin fluctuates between the spin 1 and spin zero. In the collaboration with the experimentalists at TU Delft we uncovered the workings of

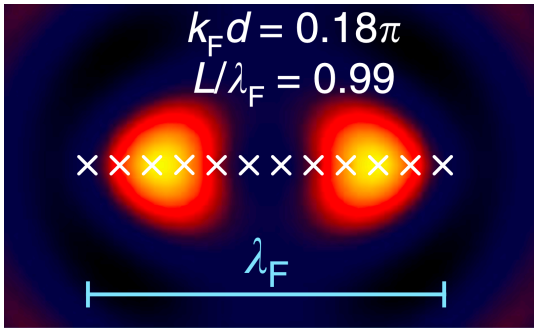

Figure 3.1: Local density of states at E_F in the 2D substrate of a multi-impurity Anderson Hamiltonian with 12 impurities (marked with crosses). The Fermi wavelength of the substrate is shown; annotated are the ratios of λ_F to the length L of the chain and the inter-atom spacing d. Reproduced from [Article 14] with permission.

the Dzyaloshinskii-Moriya interaction (1.11) in a two-spin all-organic radical [Article 15], showing an unconventional temperature dependence of the conductance.

3.4 Quantum size-effects in atomic Kondo chains

In Chapter 2 I explored quantum size effects in molecular chains. These weakly-correlated systems were described fairly well by an effectively independent-particle theory. But what happens when the 'repeating unit' becomes a Kondo impurity?

I addressed this question with D. Serrate, M. Moro and co-authors in [Article 14]. My experimental colleagues built fascinating linear chains of magnetic ad-atoms (Co) on the metallic surface Ag(111). The starting point for my theory was therefore the model of Sec. 1.2.3. In the limit $M \to \infty$, the model represents a specific form of an Anderson lattice: the Anderson impurities are one-dimensional, but the host metal is 3D [14]. When the impurities are in the Coulomb-blockade limit, the Anderson lattice exhibits competition between a collective Kondo screening (Fermi liquid state) and magnetic correlations induced by an RKKY mechanism. When collective Kondo screening is the winner, an impurity quasiparticle band forms. If such Kondo chains are made finite, quantum size-effects could reveal the emergence of the quasiparticle band from out of the single-impurity.

To explore this, I calculated the local density of states (LDOS) using many-body perturbation theory for the multi-impurity Anderson Hamiltonian described in Sec. 1.2.3. In the Kondo-screened regime, the LDOS shows Kondo peaks whose amplitude fluctuates along the chain with a typical scale λ_F, *i.e.* the Fermi wavelength. Fig. 3.1 shows a typical calculated local density of states in the substrate (see

Eq. (1.15) and below) with two peaks and spatial modulations at the scale λ_F. The origin of this modulation lies in the substrate-mediated hybridization (see Sec. 1.2.3). My calculations further demonstrated that the Kondo resonances are enhanced at the edges of the chain for chains with length $\sim \lambda_F$, but not for shorter chains. The theoretical results are in agreement with the experimental analysis (STM).

This quantum size-effect is imposed by the Fermi surface of the host metal. It does not show features intrinsic to the chain, in contrast with, *e.g.* the Oac from Sec. 2.3.1. Theoretically, we could expect a change in the behavior for longer chains, namely, a formation of a quasiparticle 1D band. In a 3D Anderson lattice, such quasiparticles are dubbed 'heavy fermions' [14].

4 Outlook

In the previous chapters I showed many examples of how electronic transport through nanoscale systems interplays with localized spins and displays effects of size-quantization. This central topic of the thesis offers several ramifications; here I mention those that address timely open questions of physics and nanosciences:

- Chirality-induced spin selective (CISS) transport
- Generation of a directed rotation at nanoscale
- Impurities on superconducting substrates.

4.1 Molecular motor

Inelastic scattering (Sec. 3.2.1) offers the possibility to transfer the angular momentum of the tunneling electron to the molecule, generating a mechanical torque. If the molecule has an axis of rotation, the possibility of a current-driven molecular motor has been explored [41, 42, 43]. I made a contribution to the field of molecular motors by employing Lagrangian dynamics to simulate the effects of a classical particle-current [Article 21]. My calculations showed that a controlled rotation can be achieved even without angular momentum being transferred. I applied the model to helical molecules, where understanding angular momentum transfer has become of vivid interest, as follows below.

4.2 Chirality-induced spin selectivity

In recent 15 years there has been an outburst of experimental works that report spin-selective phenomena in helical molecules. These results are unexpected and puzzling because reported molecules (oligomers) are non-magnetic and have weak spin-orbit effects [44].

Analytic calculation of spin conductances of helical molecules, described by a minimal model with spin-orbit coupling, was done by me and presented with co-authors in [Article 23]. My results predict a peculiar consequence of time-reversal invariance for spin transport: An application of voltage bias across such molecules leads to a parallel magnetizing of the two contacts. This work extends an earlier work of us which dealt with spin-relaxation rates in a model helical molecule [Article 19].

4.3 Impurities on superconductors

The quest for designing atomic-scale qubits has been a strong motivation to explore quantum impurities on superconductors [45, 46]. In these quantum impurities, Majorana modes and Yu-Shiba-Rusinov states play an important role.

4.3.1 Majorana modes

Majorana modes are of interest for potential applications because they are topologically protected [47]. My calculations explored the consequences of coupling a Majorana mode to a resonant level [Article 2].

4.3.2 Inelastic vibrational transitions coupled to a Yu-Shiba-Rusinov state

A resonant level from the previous paragraph could represent a molecule; however, as I have emphasized in this thesis, molecules can host spin and vibrational excitations as well. In a certain parametric regime, a so-called Yu-Shiba-Rusinov resonance results from an interaction of a localized spin with the superconducting host [48]. If the spin is localized in a molecular adsorbate, the scanning-tunneling current can detect a plethora of vibrational excitations, as shown in the group of Richard Berndt [49]. I have collaborated with A. Koliogiorgos to devise a method to calculate the respective vibrational spectrum from first principles [Article 24].

5 Conclusions

My habilitation thesis offers some natural conclusions, which I briefly state below. I would like to emphasize, that these ideas reflect the development of the whole field in the years 2011–2023, and my conclusions express my personal view on this development.

Nanoscale contacts offer a wide range of theoretical approaches to be applied. From atomistic DFT calculations, through model Hamiltonians and associated many-body techniques, classical dynamics to scattering theory. It should be emphasized that even the most detailed atomistic description cannot deliver quantitative agreement with the measurements. This seems to be the case also with the promising *GW* approximation, as argued in [Article 25]. The lack of quantitative agreement is by no means a hurdle, for a wealth of qualitative and model-based understanding has been gained in these complex systems.

An example of such qualitative understanding was given: In the topic of quantum size-effects, my works pointed out the connection between band theory and the length-dependent conductance (or gap). The question to what extent will band-structure effects influences the gaps of oligoacenes on gold remains open. Essentially it boils down to the extent correlation effects become screened on the surface, a question of fundamental importance.

For magnetic molecules displaying correlated Kondo behavior, my works revealed how internal molecular structure (spin and vibrational excitations) influences the transport spectroscopy. Furthermore, I have shown that DFT based calculations, if interpreted correctly, can guide the subsequent selection and design of an appropriate spin Hamiltonian.

Although my work is not primarily aimed at technological applications, I believe that the knowledge gained on molecular junctions and nanoscale spin devices - contributed to by this thesis - can positively inspire the design of new materials and devices.

List of Associated Publications

[Article 1] R. Korytár, N. Lorente, and J.-P. Gauyacq. "Many-body effects in magnetic inelastic electron tunneling spectroscopy". In: *Phys. Rev. B* 85 (12 2012), p. 125434. DOI: 10.1103/PhysRevB.85.125434.

[Article 2] R. Korytár and P. Schmitteckert. "Probing Majorana modes in the tunneling spectra of a resonant level". In: *J. Phys.: Condens. Matter* 25.47 (2013), p. 475304. DOI: 10.1088/0953-8984/25/47/475304.

[Article 3] R. Korytár and F. Evers. "Spin locking at the apex of nano-scale platinum tips". In: *Surf. Sci.* 618 (2013), pp. 49–52. DOI: 10.1016/j.susc.2013.09.008.

[Article 4] T. Yelin, R. Vardimon, N. Kuritz, R. Korytár, A. Bagrets, F. Evers, L. Kronik, and O. Tal. "Atomically wired molecular junctions: Connecting a single organic molecule by chains of metal atoms". In: *Nano Lett.* 13.5 (2013), pp. 1956–1961. DOI: 10.1021/nl304702z.

[Article 5] D. Rakhmilevitch, R. Korytár, A. Bagrets, F. Evers, and O. Tal. "Electron-vibration interaction in the presence of a switchable Kondo Resonance realized in a molecular junction". In: *Phys. Rev. Lett.* 113 (23 2014). Editor's Suggestion, p. 236603. DOI: 10.1103/PhysRevLett.113.236603.

[Article 6] R. Korytár, D. Xenioti, P. Schmitteckert, M. Alouani, and F. Evers. "Signature of the Dirac cone in the properties of linear oligoacenes". In: *Nature Commun.* 5.1 (2014), p. 5000. DOI: 10.1038/ncomms6000.

[Article 7] P. Schnäbele, R. Korytar, A. Bagrets, T. Roman, T. Schimmel, A. Groß, and F. Evers. "Ab initio transport calculations for single-atom copper junctions in the presence of hydrogen chloride". In: *J. Phys. Chem. C* 118.48 (2014), pp. 28252–28257. DOI: 10.1021/jp5093898.

[Article 8] L. Zhang et al. “Kondo effect in binuclear metal-organic complexes with weakly interacting spins”. In: *Phys. Rev. B* 91 (19 2015), p. 195424. DOI: 10.1103/PhysRevB.91.195424.

[Article 9] O. Adak, R. Korytár, A. Joe, F. Evers, and L. Venkataraman. “Impact of electrode density of states on transport through Pyridine–linked single molecule junctions”. In: *Nano Lett.* 15 (2015), pp. 3716–3722. DOI: 10.1021/acs.nanolett.5b01195.

[Article 10] T. Yelin, R. Korytár, N. Sukenik, R. Vardimon, B. Kumar, C. Nuckolls, F. Evers, and O. Tal. “Conductance saturation in a series of highly transmitting molecular junctions”. In: *Nature Mater.* 15 (2016), pp. 444–449. DOI: 10.1038/nmat4552.

[Article 11] H. Li et al. “Silver makes better electrical contacts to thiol-terminated silanes than gold”. In: *Angew. Chem., Int. Ed. Engl.* 56.45 (2017), pp. 14145–14148. DOI: 10.1002/anie.201708524.

[Article 12] P. Schmitteckert, R. Thomale, R. Korytár, and F. Evers. “Incommensurate quantum-size oscillations in acene-based molecular wires—Effects of quantum fluctuations”. In: *J. Chem. Phys.* 146.9 (2017). DOI: 10.1063/1.4975319.

[Article 13] M. J. van Setten, D. Xenioti, M. Alouani, F. Evers, and R. Korytár. “Incommensurate quantum size oscillations of oligoacene wires adsorbed on Au (111)”. In: *J. Phys. Chem. C* 123.14 (2019), pp. 8902–8907. DOI: 10.1021/acs.jpcc.8b12213.

[Article 14] M. Moro-Lagares, R. Korytár, M. Piantek, R. Robles, N. Lorente, J. I. Pascual, M. R. Ibarra, and D. Serrate. “Real space manifestations of coherent screening in atomic scale Kondo lattices”. In: *Nature Commun.* 10.1 (2019), p. 2211. DOI: 10.1038/s41467-019-10103-5.

[Article 15] P. Zalom, J. de Bruijckere, R. Gaudenzi, H. S. J. van der Zant, T. Novotný, and R. Korytár. “Magnetically tuned Kondo effect in a molecular double quantum dot: Role of the anisotropic exchange”. In: *J. Phys. Chem. C* 123.18 (2019), pp. 11917–11925. DOI: 10.1021/acs.jpcc.9b00783.

[Article 16] A. García et al. “Siesta: Recent developments and applications”. In: *J. Chem. Phys.* 152.20 (2020), p. 204108. DOI: 10.1063/5.0005077.

[Article 17] F. Evers, R. Korytár, S. Tewari, and J. M. van Ruitenbeek. "Advances and challenges in single-molecule electron transport". In: *Rev. Mod. Phys.* 92.3 (2020), p. 035001. DOI: 10.1103/RevModPhys.92.035001.

[Article 18] M. Žonda et al. "Resolving ambiguity of the Kondo temperature determination in mechanically tunable single-molecule Kondo systems". In: *J. Phys. Chem. Lett.* 12.27 (2021), pp. 6320–6325. DOI: 10.1021/acs.jpclett.1c01544.

[Article 19] J. M. van Ruitenbeek, R. Korytár, and F. Evers. "Chirality-controlled spin scattering through quantum interference". In: *J. Chem. Phys.* 159.2 (2023), p. 024710. DOI: 10.1063/5.0156316.

[Article 20] V. Varade et al. "Chiral light emission from a hybrid magnetic molecule–monolayer transition metal dichalcogenide heterostructure". In: *ACS Nano* 17.3 (2023), pp. 2170–2181. DOI: 10.1021/acsnano.2c08320.

[Article 21] R. Korytár and F. Evers. "Current-induced mechanical torque in chiral molecular rotors". In: *Beilstein Journal of Nanotechnology* 14 (2023), pp. 711–721. DOI: 10.3762/bjnano.14.57.

[Article 22] B. Pabi, J. Šebesta, R. Korytár, O. Tal, and A. N. Pal. "Structural regulation of mechanical gating in molecular junctions". In: *Nano Lett.* 23.9 (2023), pp. 3775–3780. DOI: 10.1021/acs.nanolett.3c00043.

[Article 23] R. Korytár, J. M. van Ruitenbeek, and F. Evers. "Spin conductances and magnetization production in chiral molecular junctions". In: *J. Chem. Phys.* 161.9 (2024), p. 094111. DOI: 10.1063/5.0226594.

[Article 24] A. Koliogiorgos and R. Korytár. "Minimal model of inelastic tunneling of vibrating magnetic molecules on superconducting substrates". In: *Phys. Rev. B* 110 (23 2024), p. 235424. DOI: 10.1103/PhysRevB.110.235424.

[Article 25] Š. Marek and R. Korytár. "Widening of the fundamental gap in cluster GW for metal–molecular interfaces". In: *Phys. Chem. Chem. Phys.* 26.3 (2024), pp. 2127–2133. DOI: 10.1039/D3CP04082H.

Bibliography

[1] E. Scheer and J. C. Cuevas. *Molecular Electronics, An Introduction to Theory and Experiment*. World Scientific, 2017.

[2] G. D. Scott and D. Natelson. "Kondo resonances in molecular devices". In: *ACS Nano* 4 (2010), pp. 3560–3579.

[3] S. V. Aradhya and L. Venkataraman. "Single-molecule junctions beyond electronic transport". In: *Nature Nanotechnol.* 8 (2013), pp. 399–410.

[4] S. Datta. *Electronic Transport in Mesoscopic Systems*. Cambridge University Press, 1997.

[5] S. Washburn. "Resistance fluctuations in small samples: Be careful when playing with Ohm's law". In: *B. Kramer (Ed.), Quantum Coherence in Mesoscopic Systems*. Plenum Press, New York, USA, 1991.

[6] C. Caroli, R. Combescot, P. Nozières, and D. Saint-James. "Direct calculation of the tunneling current". In: *J. Phys. C: Solid State Phys.* 4 (1971), p. 916.

[7] F. Pauly, J. K. Viljas, U. Huniar, M. Häfner, S. Wohlthat, J. Bürkle, J. C. Cuevas, and G. Schön. "Cluster-based density-functional approach to quantum transport through molecular and atomic contacts". In: *New J. Phys.* 10 (2008), p. 125019.

[8] A. Arnold, F. Weigend, and F. Evers. "Quantum chemistry calculations for molecules coupled to reservoirs: Formalism, implementation and application to benzene-dithiol". In: *J. Chem. Phys.* 126 (2007), p. 174101.

[9] M. Brandbyge, J.-L. Mozos, P. Ordejón, J. Taylor, and K. Stokbro. "Density-functional method for nonequilibrium electron transport". In: *Phys. Rev. B* 65 (2002), p. 165401.

[10] A. Bagrets. "Spin-polarized electron transport across metal–organic molecules: A density functional theory approach". In: *J. Chem. Theory Comput.* 9.6 (2013), pp. 2801–2815. DOI: 10.1021/ct4000263.

[11] P. W. Anderson. "Localized magnetic states in metals". In: *Phys. Rev.* 124 (1961), p. 41.

[12] G. D. Mahan. *Many-Particle Physics*. Springer Science & Business Media, 2013.

[13] J. R. Schrieffer and P. A. Wolff. "Relation between the Anderson and Kondo Hamiltonians". In: *Phys. Rev.* 149.2 (1966), p. 491.

[14] P. Coleman. *Introduction to Many-Body Physics*. Cambridge University Press, 2015.

[15] S. Alexander and P. W. Anderson. "Interaction between localized states in metals". In: *Phys. Rev.* 133 (1964), A1594.

[16] M. Pustilnik, Y. Avishai, and K. Kikoin. "Quantum dots with even number of electrons: Kondo effect in a finite magnetic field". In: *Phys. Rev. Lett.* 84 (8 2000), p. 1756. DOI: 10.1103/PhysRevLett.84.1756.

[17] M. Pustilnik and L. Glazman. "Kondo effect induced by a magnetic field". In: *Phys. Rev. B* 64.4 (2001), p. 045328.

[18] K. Yosida. *Theory of Magnetism*. Springer Series in Solid-State Sciences. Springer Berlin Heidelberg, 1996.

[19] A. C. Hewson. *The Kondo Problem to Heavy Fermions*. Cambridge studies in magnetism. Cambridge University Press, 1993.

[20] P. W. Anderson. *Basic Notions Of Condensed Matter Physics*. CRC Press, 1994.

[21] M. L. Perrin et al. "Large tunable image-charge effects in single-molecule junctions". In: *Nature Nanotechnol.* 8 (2013), pp. 282–287.

[22] J. R. Quinn, F. W. Foss, L. Venkataraman, M. S. Hybertsen, and R. Breslow. "Single-molecule junction conductance through diaminoacenes". In: *J. Am. Chem. Soc.* 129 (2007), pp. 6714–6715.

[23] T. A. Su, M. Neupane, M. L. Steigerwald, L. Venkataraman, and C. Nuckolls. "Chemical principles of single-molecule electronics". In: *Nature Reviews Materials* 1.3 (2016), pp. 1–15.

[24] S. Kivelson and O. Chapman. “Polyacene and a new class of quasi-one-dimensional conductors”. In: *Phys. Rev. B* 28.12 (1983), p. 7236.

[25] H. F. Bettinger. “Electronic structure of higher acenes and polyacene: The perspective developed by theoretical analyses”. In: *Pure and Applied Chemistry* 82.4 (2010), pp. 905–915.

[26] C. Tönshoff and H. F. Bettinger. “Pushing the limits of acene chemistry: The recent surge of large acenes”. In: *Chemistry–A European Journal* 27.10 (2021), pp. 3193–3212.

[27] F. Eisenhut et al. “Dodecacene generated on surface: Reopening of the energy gap”. In: *ACS Nano* 14.1 (2020), pp. 1011–1017. DOI: 10.1021/acsnano.9b08456.

[28] J. Krüger et al. “Imaging the electronic structure of on-surface generated hexacene”. In: *Chem. Commun.* 53.10 (2017), pp. 1583–1586.

[29] Z. Ruan, J. Schramm, J. B. Bauer, T. Naumann, H. F. Bettinger, R. Tonner-Zech, and J. M. Gottfried. “Synthesis of tridecacene by multistep single-molecule manipulation”. In: *J. Am. Chem. Soc.* 146.6 (2024), pp. 3700–3709. DOI: 10.1021/jacs.3c09392.

[30] P. Fulde. *Electron Correlations in Molecules and Solids*. Vol. 100. Springer Science & Business Media, 2012.

[31] R. Zuzak et al. “On-surface synthesis and determination of the open-shell singlet ground state of tridecacene”. In: *Angew. Chem., Int. Ed. Engl.* 63.9 (2024), e202317091.

[32] R. Requist, P. P. Baruselli, A. Smogunov, M. Fabrizio, S. Modesti, and E. Tosatti. “Metallic, magnetic and molecular nanocontacts”. In: *Nature Nanotechnology* 11.6 (2016), pp. 499–508.

[33] F. Strigl, C. Espy, M. Bückle, E. Scheer, and T. Pietsch. “Emerging magnetic order in platinum atomic contacts and chains”. In: *Nature Commun.* 6.1 (2015), p. 6172.

[34] A. Smogunov, A. Dal Corso, and E. Tosatti. “Magnetic phenomena, spin-orbit effects, and Landauer conductance in Pt nanowire contacts: Density-functional theory calculations”. In: *Phys. Rev. B* 78 (1 2008), p. 014423. DOI: 10.1103/PhysRevB.78.014423.

[35] N. Lorente and M. Persson. “Theory of single molecule vibrational spectroscopy and microscopy”. In: *Phys. Rev. Lett.* 85.14 (2000), p. 2997.

[36] N. Lorente and M. Brandbyge. “Theory of elastic and inelastic transport from tunneling to contact”. In: *Scanning Probe Microscopies Beyond Imaging*. John Wiley & Sons, Ltd, 2006. Chap. 15, pp. 469–507. DOI: https://doi.org/10.1002/3527608516.ch15.

[37] R. Korytár and N. Lorente. “Multi-orbital non-crossing approximation from maximally localized Wannier functions: the Kondo signature of copper phthalocyanine on Ag (100)”. In: *J. Phys.: Condens. Matter* 23 (2011), p. 355009.

[38] A. Mugarza, R. Robles, C. Krull, R. Korytár, N. Lorente, and P. Gambardella. “Electronic and magnetic properties of molecule-metal interfaces: Transition-metal phthalocyanines adsorbed on Ag(100)”. In: *Phys. Rev. B* 85 (15 2012), p. 155437.

[39] M. Galpin and D. Logan. “A local moment approach to the gapped Anderson model”. In: *Eur. Phys. J. B* 62 (2008), pp. 129–145.

[40] R. Žitko, R. Peters, and T. Pruschke. “Properties of anisotropic magnetic impurities on surfaces”. In: *Phys. Rev. B* 78.22 (2008), p. 224404.

[41] G. J. Simpson, V. García-López, A. Daniel Boese, J. M. Tour, and L. Grill. “How to control single-molecule rotation”. In: *Nature Commun.* 10.1 (2019), pp. 1–6.

[42] F. Eisenhut et al. “One-way rotation of a chemically anchored single molecule-rotor”. In: *Nanoscale* 13.38 (2021), pp. 16077–16083.

[43] T. Jasper-Toennies, M. Gruber, S. Johannsen, T. Frederiksen, A. Garcia-Lekue, T. Jäkel, F. Roehricht, R. Herges, and R. Berndt. “Rotation of ethoxy and ethyl moieties on a molecular platform on Au (111)”. In: *ACS Nano* 14.4 (2020), pp. 3907–3916.

[44] F. Evers et al. “Theory of chirality induced spin selectivity: Progress and challenges”. In: *Advanced Materials* 34.13 (2022), p. 2106629.

[45] R. Žitko. “Superconducting quantum dot and the sub-gap states”. In: *Spintronics XI*. Ed. by H. Jaffrès, H.-J. Drouhin, J.-E. Wegrowe, and M. Razeghi. arXiv:1901.01039. SPIE, 2018, p. 58. DOI: 10.1117/12.2322365.

[46] D.-J. Choi, N. Lorente, J. Wiebe, K. Von Bergmann, A. F. Otte, and A. J. Heinrich. “Colloquium: Atomic spin chains on surfaces”. In: *Rev. Mod. Phys.* 91.4 (2019), p. 041001.

[47] S. R. Elliott and M. Franz. “Colloquium: Majorana fermions in nuclear, particle, and solid-state physics”. In: *Rev. Mod. Phys.* 87.1 (2015), pp. 137–163.

[48] A. V. Balatsky, I. Vekhter, and J.-X. Zhu. “Impurity-induced states in conventional and unconventional superconductors”. In: *Rev. Mod. Phys.* 78.2 (2006), pp. 373–433.

[49] J. Homberg, A. Weismann, T. Markussen, and R. Berndt. “Resonance-enhanced vibrational spectroscopy of molecules on a superconductor”. In: *Phys. Rev. Lett.* 129.11 (2022), p. 116801.

Associated publications (copies)

The associated publications are enclosed in the long version, only.